iScience

CellPress
OPEN ACCESS

Article

Leishmania mexicana promotes pain-reducing metabolomic reprogramming in cutaneous lesions

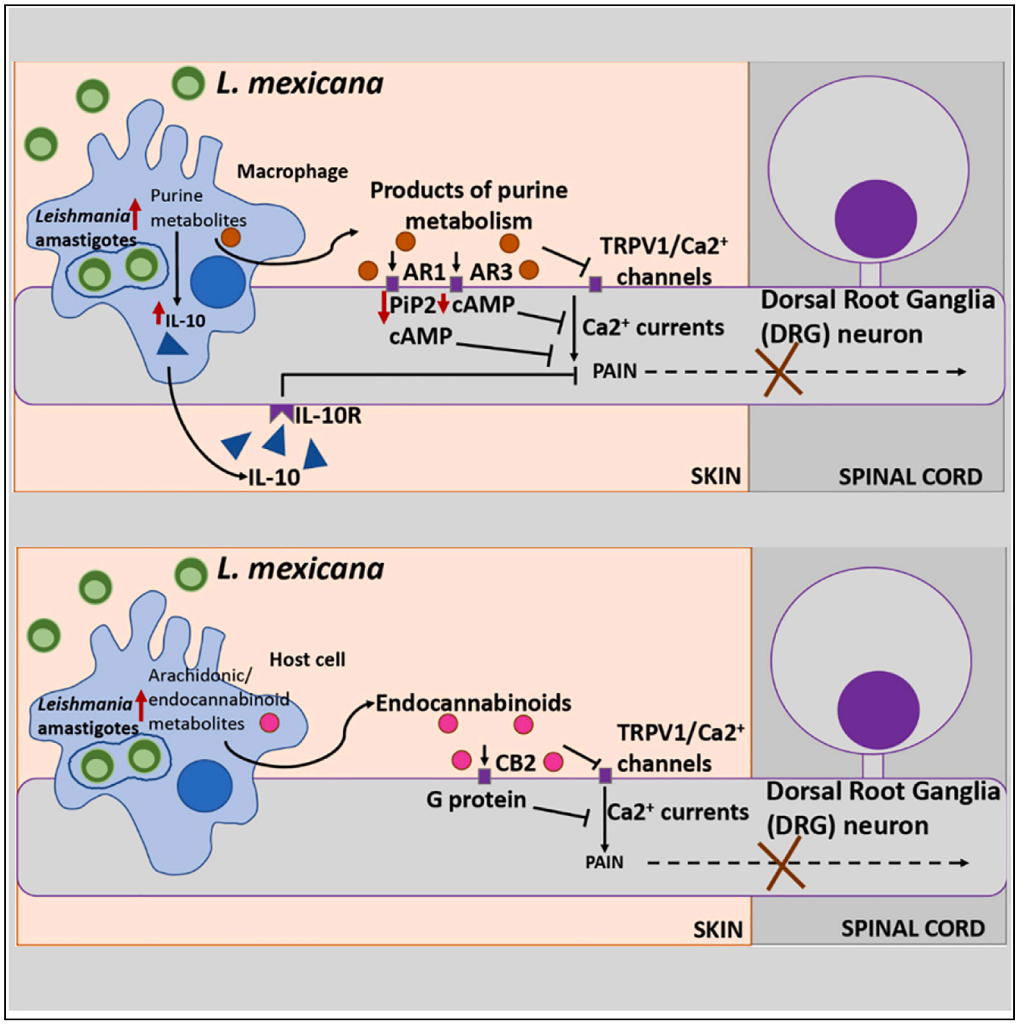

Greta Volpedo, Timur Oljuskin, Blake Cox, ..., Hira L. Nakhasi, Sreenivas Gannavaram, Abhay R. Satoskar

abhay.satoskar@osumc.edu

Highlights

L. mexicana infection triggers anti-nociceptive pathways in the infected tissue

L. mexicana induces upregulation of anti-inflammatory and anti-nociceptive purines

L. mexicana promotes anti-nociceptive arachidonic acid and endocannabinoid metabolism

These metabolic signatures may contribute to the lack of pain in CL lesions

Volpedo et al., iScience *26*, 108502
December 15, 2023
https://doi.org/10.1016/j.isci.2023.108502

iScience

CellPress
OPEN ACCESS

Article

Leishmania mexicana promotes pain-reducing metabolomic reprogramming in cutaneous lesions

Greta Volpedo,[1,2] Timur Oljuskin,[3] Blake Cox,[2] Yulian Mercado,[2] Candice Askwith,[4] Nazli Azodi,[5] Matthew Bernier,[6] Hira L. Nakhasi,[5] Sreenivas Gannavaram,[5] and Abhay R. Satoskar[1,2,7,*]

SUMMARY

Cutaneous leishmaniasis (CL) is characterized by extensive skin lesions, which are usually painless despite being associated with extensive inflammation. The molecular mechanisms responsible for this analgesia have not been identified. Through untargeted metabolomics, we found enriched anti-nociceptive metabolic pathways in *L. mexicana*-infected mice. Purines were elevated in infected macrophages and at the lesion site during chronic infection. These purines have anti-inflammatory and analgesic properties by acting through adenosine receptors, inhibiting TRPV1 channels, and promoting IL-10 production. We also found arachidonic acid (AA) metabolism enriched in the ear lesions compared to the non-infected controls. AA is a metabolite of anandamide (AEA) and 2-arachidonoylglycerol (2-AG). These endocannabinoids act on cannabinoid receptors 1 and 2 and TRPV1 channels to exert anti-inflammatory and analgesic effects. Our study provides evidence of metabolic pathways upregulated during *L. mexicana* infection that may mediate anti-nociceptive effects experienced by CL patients and identifies macrophages as a source of these metabolites.

INTRODUCTION

Cutaneous leishmaniasis (CL) is caused by the protozoan parasite *Leishmania* and it is the most common form of the disease with an incidence of 1 million new cases every year.[1,2] Depending on the causative species, the clinical manifestations of CL can range from self-healing skin lesions to diffused ulcers that can persist for months and require treatment.[3] *L. mexicana* is a New World CL strain pervasive in Central and South America, which can cause chronic non-healing skin lesions on different parts of the body.[4,5] Interestingly, CL lesions, including those caused by *L. mexicana*, are usually painless in humans,[6–8] a clinical phenomenon that has not received much attention from the scientific community. This is an intriguing phenotype as inflammatory lesions, such as lesions caused by *Staphylococcus aureus*,[9] *Herpes* virus,[10] and *Varicella zoster* virus,[11] are generally painful. CL lesions can range between 0.5 and 3 cm in diameter[12] and present with chronic inflammation and infiltration of lymphocytes, plasma cells, and macrophages.[13,14] Despite the inflammation, CL lesions are usually painless, indicating that *Leishmania* infection may trigger anti-nociceptive activities in the infected tissues. Interestingly, pain is reported in human CL lesions after secondary bacterial infections, which are common following ulceration.[12,15] This suggests that any mediators preventing pain produced in the primary lesions are overridden by other signals following a secondary infection, and that nociception at the lesion site might be due to a pathogen-specific mechanism. Interestingly, CL infections seem to be painless from the sand fly blood meal to the development and progression of the lesions,[6–8] which could indicate an intricate host-parasite interaction that may favor the establishment and spread of infection. Analgesia could delay the infected individual from seeking medical attention, allowing for the infection to establish and spread to other areas of the body and to other individuals via the sand fly vector. This suggests that there might be a broader biological advantage in having painless invasion and painless lesions. For these reasons, it is imperative to continue exploring this understudied phenomenon to elucidate the molecular mechanisms causing lack of pain at the lesion site. Several studies have been conducted in mice infected with *L. major*, an Old World cutaneous strain, to explore the role of cytokines in CL-mediated analgesia,[16–21] as it is well established that these mediators can modulate pain at the neural level. Nociceptive neurons express cytokine receptors, which can modulate neuronal excitability and pain signaling.[22] For instance, interleukin (IL)-10, IL-13, and IL-4 are cytokines produced in *Leishmania* susceptible models and are known to have analgesic properties.[6] On the other hand, pro-inflammatory cytokines have been shown to cause pain by increasing excitability of nociceptive neurons.[23] However, studies focusing on the role of cytokines in *L. major*-mediated anti-nociception have shown contradicting results

[1]Department of Microbiology, The Ohio State University, Columbus, OH 43210, USA
[2]Department of Pathology, Wexner Medical Center, The Ohio State University, Columbus, OH 43210, USA
[3]Animal Parasitic Disease Lab, Agricultural Research Service, USDA, Beltsville, MD, USA
[4]Department of Neuroscience, The Ohio State University, Columbus, OH 43210, USA
[5]Division of Emerging and Transfusion Transmitted Diseases, CBER, FDA, Silver Spring, MD, USA
[6]Mass Spectrometry and Proteomics Facility, The Ohio State University, Columbus, OH 43210, USA
[7]Lead contact
*Correspondence: abhay.satoskar@osumc.edu
https://doi.org/10.1016/j.isci.2023.108502

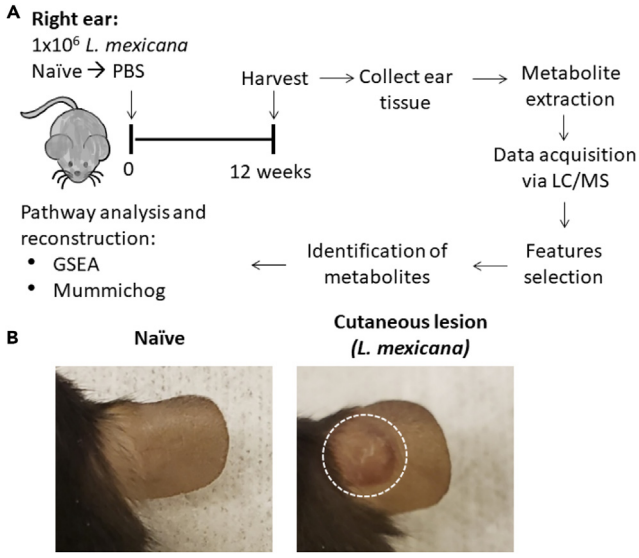

Figure 1. Experimental design for metabolomic analysis to detect mediators of analgesic activity following *L. mexicana* infection

(A) Experimental design of infection, sample collection, and analysis.

(B) Representative images of the ears of naive (n = 2) and *L. mexicana*-infected (n = 4) mice at 12 weeks post infection. Abbreviations: LC/MS: liquid chromatography/mass spectrometry; GSEA: gene set enrichment analysis.

in pre-clinical models.[16–21] Even when analgesia was observed, changes in the expression of cytokines alone did not seem to be responsible for this phenotype.[16] These observations led us to hypothesize that other non-immunological mediators produced or upregulated during *Leishmania* infection may directly mediate anti-nociception at the lesion site. For instance, different metabolites have been previously explored for their analgesic roles. In particular, endocannabinoids,[24] protectins,[25,26] maresins,[27,28] resolvins,[28] and lipoxins,[29] among others, have been shown to have anti-nociceptive properties by directly acting on nociceptor neurons. In order to acquire a complete and unbiased understanding of the mediators produced during infection, we used an untargeted metabolomics approach to identify *Leishmania*-induced mediators with analgesic properties. Furthermore, we investigated pain responses during.

Furthermore, we investigated pain responses during *L. mexicana* infection, prevalent in geographically distinct endemic areas and presenting different disease immunology and pathology compared to *L. major*.[30–33] In particular, *L. mexicana* lesions are not self-resolving,[4,5] contrary to *L. major* lesions, and would require a prolonged analgesic action.

In this study, we show that mice infected with *L. mexicana* display enriched metabolites with anti-nociceptive properties at the infected tissue. In particular, endogenous purines, arachidonic acid (AA), and endocannabinoid metabolites were upregulated in the lesions of *L. mexicana*-infected mice compared to their uninfected controls and could lead to the lack of pain observed in CL patients. Exploring the metabolic-neuro-immune interaction in CL, with a particular focus on macrophages and nociceptive neurons, could elucidate the anti-nociceptive mechanism/s leading to analgesia in CL patients.

RESULTS

L. mexicana infection results in metabolic differences compared to naive skin tissue

In order to gain a comprehensive understanding of the mediators produced during infection, as well as those that might play a role in *L. mexicana*-mediated anti-nociception, we performed untargeted mass spectrometry on the ear lesions of C57BL/6 mice chronically infected intradermally with *L. mexicana* (Figure 1A). Our goal was to screen for enrichment of mediators with known anti-nociceptive properties in infected, compared to non-infected ear tissue. Figure 1B shows representative images of the ears of naive and *L. mexicana*-infected mice at harvest. As expected, infected mice showed a large lesion at 12 weeks post infection, indicated by a white dotted circle (Figure 1B). Using volcano plots (Figures 2A and 2B), we selected significant features from the positive and negative modes of mass spectrometry analysis. The peaks identified with the positive mode most commonly correspond to protonated molecules, while those identified with the negative mode typically correspond to deprotonated analytes. A fold change (FC) threshold (x) 2 and t tests threshold (y) 0.05 were set for the volcano plots (Figures 2A and 2B). We have also used partial least squares-discriminant analysis (PLS-DA), a supervised multivariate analytic approach, to identify molecular pathways enriched during *L. mexicana* infection (Figures 2C and 2D). The high level of similarity between R2 and Q2 values in both positive (Figure 2E) and negative (Figure 2F) mode datasets indicated that the model is not overfitted to the data. Additionally, unsupervised clustering by principal-component analysis (PCA) of both positive (Figure 2G) and negative (Figure 2H) mode datasets showed clear differentiation of the data into two distinct clusters. Our analysis revealed distinct metabolic signatures in the ear tissue of naive, compared to infected mice, highlighting a significant *Leishmania* infection-associated metabolic shift.

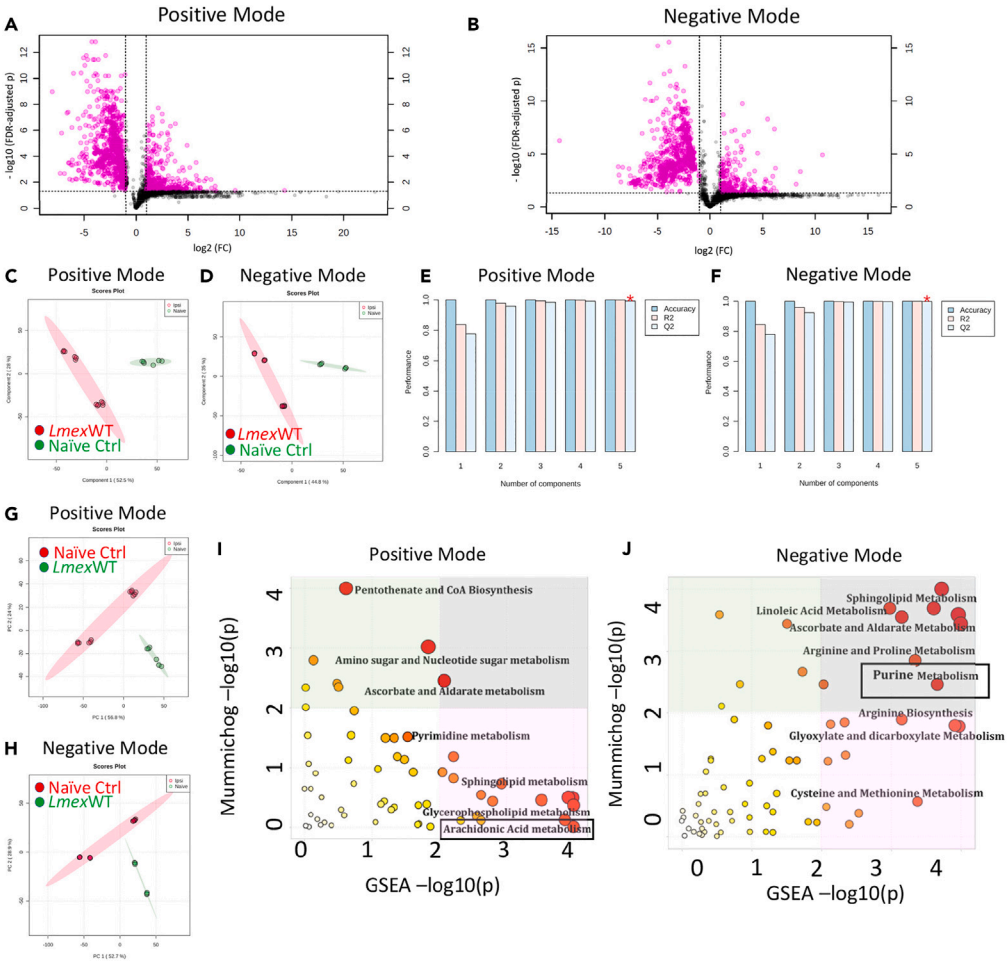

Figure 2. Infection with *L. mexicana* leads to enriched purine and arachidonic acid metabolism in cutaneous lesions

Normalized data from ear tissues of C57BL/6 mice infected with *L. mexicana* (12 weeks post infection) and naive controls were used to perform statistical analysis. Features selected by volcano plot from positive (A) and negative (B) modes of LC/MS with log-transformed fold change threshold (2-fold, x-axis) and t-tests threshold (0.05, y axis). Score plots between the selected PLS-DA from positive (C) and negative (D) modes are shown. To measure the accuracy of the PLS-DA model, the plots for the R2 and Q2 values of the positive (E) and negative (F) modes are shown. Score plots from the selected PCA from positive (G) and negative (H) modes are also shown. The Integrated MS Peaks to Paths plot summarizes the results of the Fisher's method for combining mummichog (y) and GSEA (x) p-values from the positive (I) and negative (J) mode datasets, showing the enriched metabolic pathways. The size and color of the circles correspond to their log-transformed combined p values. Large and red circles are considered the most perturbed pathways. The colored areas show the significant pathways based on either GSEA (pink) or mummichog (green), and the purple area in the upper right quadrant highlights significant pathways identified by both algorithms. Highlighted by a black box are arachidonic acid metabolism (I), and purine metabolism (J).

L. mexicana infection leads to enrichment of purine metabolites with anti-nociceptive activity *in vivo*

In order to identify specific anti-nociceptive metabolic pathways enriched in infected tissues, we used both mummichog and Gene Set Enrichment Analysis (GSEA) analysis. Mummichog analysis uses an algorithm that predicts functional activity bypassing metabolite identification, while GSEA requires the metabolites to be identified before pathway/network analysis. We used the Integrated MS Peaks to Pathways plot to summarize the results of the Fisher's method for combining mummichog (y) and GSEA (x) p values from the positive and negative mode datasets, which showed several enriched pathways at the lesion site (Figures 2I and 2J). In particular, the negative mode dataset (Figure 2J) showed enriched purine metabolism in infected vs. uninfected mice (Figure 2J). Based on the t-scores for the matched metabolites, purine metabolism was found to be upregulated in infected tissues. Further investigating this pathway, we found that several purine metabolites, including those with known anti-nociceptive activities were highly upregulated during infection. In particular, xanthine, hypoxanthine, and inosine were enriched in the infected group, as identified in an integrative network analysis performed using Metscape (Figures 3A and 3B). Additionally, other purine metabolites such as xanthosine and 5-hydroxyisourate were also upregulated, while guanine and adenine were downregulated (Figure 3A). Purine metabolites have been previously implicated in anti-nociception and could therefore mediate the lack of pain reported by CL patients. Our initial mass spectrometric run identified several isoforms of the

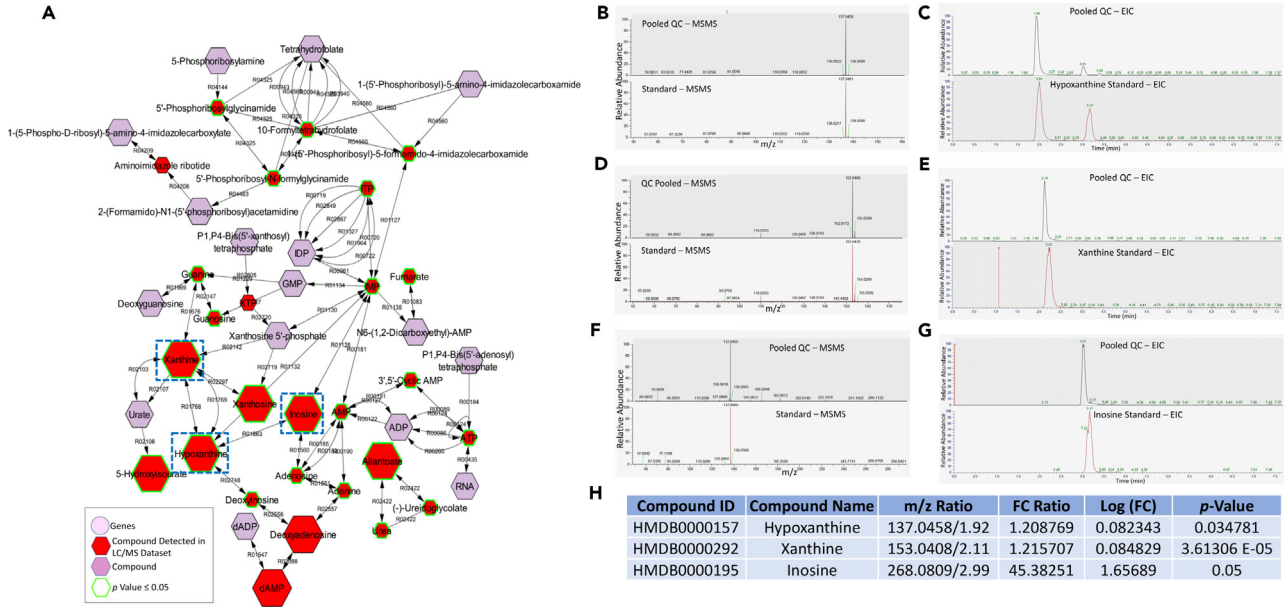

Compound ID	Compound Name	m/z Ratio	FC Ratio	Log (FC)	*p*-Value
HMDB0000157	Hypoxanthine	137.0458/1.92	1.208769	0.082343	0.034781
HMDB0000292	Xanthine	153.0408/2.11	1.215707	0.084829	3.61306 E-05
HMDB0000195	Inosine	268.0809/2.99	45.38251	1.65689	0.05

Figure 3. Infection with *L. mexicana* leads to alteration of purine metabolism

Normalized data from ear tissues of C57BL/6 mice infected with *L. mexicana* (12 weeks post infection) and naive controls were used to perform integrative compound-compound network analysis with Metscape (A). An integrative network depicting the relationship between the products of purine metabolism is shown. 10-formyltetrahydrofolate, and other non-purine metabolites upstream of purine synthesis, are also included in the network. Larger hexagons represent up-regulation, while smaller hexagons represent down-regulation. Red hexagons represent compounds detected in the dataset, while hexagons with a green outline represent statistically significant change ($p \leq 0.05$). The graph shows that infection with *L. mexicana* leads to the alteration of purine metabolism towards the enrichment of inosine, xanthine, and hypoxanthine, all of which possess anti-nociceptive activities; highlighted in the graph with a dotted blue outline. To confirm the annotation of the purine metabolites with known anti-nociceptive activities, the ear tissue extracts of infected and naive control were used to perform an untargeted LC/MS analysis alongside known standards to distinguish the isoform of the observed metabolites. Spectra depicting the fragment masses and the corresponding extracted ion chromatogram (EIC) that confirm matching patterns between sample metabolites and the known standards are shown for hypoxanthine (B–C), xanthine (D–E), and inosine (F–G). The confirmed m/z ratio, log fold change and corresponding p values of the validated metabolites (H) are shown.

purine metabolites with similar m/z ratios. To definitively confirm the annotation of the purine metabolites with known anti-nociceptive activities, such as xanthine, hypoxanthine, and inosine, ear tissue extracts from the infected and naive control tissues were used to perform a targeted LC/MS analysis alongside known standards to distinguish the isoforms of the metabolites. Spectra depicting the fragment masses (MS/MS) and the corresponding extracted ion chromatograms created by plotting the intensity of the signal observed at chosen m/z value for hypoxanthine (Figures 3B and 3C), xanthine (Figures 3D and 3E), and inosine (Figures 3F and 3G) showed a matching pattern between sample metabolites and the known standards. The fold enrichment of these validated purine metabolites along with HMDB IDs, observed m/z ratios, and associated p values indicated that anti-nociceptive purine metabolites are enriched in the infected tissues (Figure 3H).

L. mexicana infection leads to enrichment of arachidonic acid and endocannabinoid metabolites with anti-nociceptive activity

Ear tissue of infected mice also revealed additional metabolic pathways with analgesic properties, such as arachidoni acid (AA) metabolism (Figure 2I). AA metabolism is closely related to endocannabinoid metabolism, known to exert potent analgesic functions.[24] In particular, we observed increased levels of diacylglycerol and monoacylglycerol, precursors of AA, phosphatidylethanolamine and phosphatidylcholine, both precursors of the endocannabinoid anandamide (AEA), and phosphatidylinositol-3-phosphate, a precursor of the endocannabinoid 2-arachidonoylglycerol (2-AG). Furthermore, we have identified via Metscape significant up-regulation of AEA (20:4), AA, 2-AG, and the AEA metabolite ethanolamine (Figures 4A and S1A), known for their analgesic properties.[24] To visualize the metabolites of AA metabolism and their precursors, the integrated network was selected to include the metabolites of glycerophospholipid metabolism, linoleate metabolism, and prostaglandin synthesis (Figure 4A). To definitively confirm the annotation of the AA metabolites with known anti-nociceptive activities, such as AA and AEA (20:4), ear tissue extracts from the infected and naive control tissues were used to perform an untargeted LC/MS analysis alongside known standards to distinguish the isoforms of the metabolites. Spectra depicting the fragment masses (MS/MS) and the corresponding extracted ion chromatograms created by plotting the intensity of the signal observed at chosen m/z value for AA (Figures 4B and 4C) and AEA (20:4, $C_{22}H_{37}NO_2$) (Figures 4D and 4E) showed a matching pattern between sample metabolites and the known standards. Additionally, we have detected a related AA metabolite $C_{20}H_{33}NO_2$ in our dataset (Figures S1B and S2). The 348 m/z feature

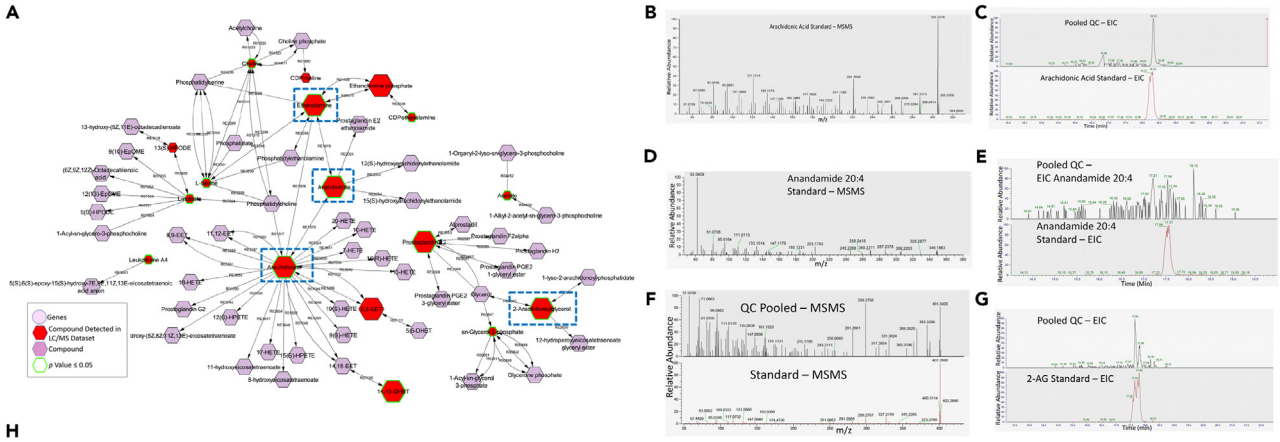

H

Compound ID	Compound Name	m/z Ratio	FC Ratio	Log (FC)	*p*-Value
HMDB0001043	Arachidonic acid	304.2399/18.31	2.564017	0.408921	5.99346E-05
HMDB0004080	Anandamide (20:4, n-3)	348.2904/17.21	8.26763998	0.917381557	0.020866291
HMDB0004666	2-Arachidoncylglycerol	378.2767/17.64	2.820739	0.450362956	0.048427925

Figure 4. Infection with *L. mexicana* leads to alteration of arachidonic acid metabolites

Normalized data from ear tissues of C57BL/6 mice infected with *L. mexicana* (12 weeks post infection) and naive controls were used to perform integrative compound-compound network analysis with Metscape. Metabolites with known anti-nociceptive activities from arachidonic acid metabolism, glycerophospholipid metabolism, linoleate metabolism, and prostaglandin formation from arachidonate are highlighted in the graph. Larger hexagons represent up-regulation, while smaller hexagons represent down-regulation. Red hexagons represent compounds detected in our dataset, while hexagons with a green outline represent statistically significant metabolites ($p \leq 0.05$). The graph shows that infection with *L. mexicana* leads to the enrichment of arachidonic acid metabolites with known anti-nociceptive activities, such as anandamide, ethanolamine, 2-arachidonylglycerol, and arachidonate; highlighted in the graph with a dotted blue outline. To confirm the annotation of arachidonic acid metabolites with known anti-nociceptive activities, the ear tissue extracts of infected and naive control were used to perform an untargeted LC/MS analysis alongside known standards to distinguish the isoform of the observed metabolites. Spectra depicting the fragment masses and the corresponding extracted ion chromatogram (EIC) that confirm matching patterns between sample metabolites and the known standards are shown for arachidonic acid (B–C), anandamide (D–E), and 2-arachidonylglycerol (F–G). The confirmed m/z ratio, log fold change and corresponding p value of the validated metabolites (H) are shown.

corresponding to AEA (20:4) standard did not match the metabolite in retention time or mass presumably due to the -C2H4 loss, thus it is reasonable to annotate this as N-acylethanolamine (NAE) 18:4. Notably, the intensity of the detection of AEA (20:4) was at a significantly lower level than that of NAE (18:4). Both AEA (20:4) and NAE 18:4 are known endocannabinoids. The fold enrichment of these validated AA metabolites along with HMDB IDs, observed m/z ratios, and associated p values indicated that anti-nociceptive AA metabolites are enriched in the infected tissues (Figure 4F).

Immortalized and primary macrophages infected with *L. mexicana* display metabolic differences compared to naive macrophages

Lesion tissues contain heterogeneous cell types, some of which may be inflammatory; however, the cellular source of the purine/AA metabolites remains unknown. In order to determine a potential cell source, we performed untargeted mass spectrometry on infected macrophages, the canonical hosts for *Leishmania* parasites. First, we used RAW 264.7 macrophages, an immortalized cell line, and then validated our results with bone marrow-derived macrophages (BMDMs), to correlate our results with physiologically relevant primary cells (Figure 5A). We selected significant features, using volcano plots with a FC threshold (x) 2 and t tests threshold (y) 0.05 from RAW 264.7 macrophages (Figures 5B and 5C) and BMDMs (Figures 5D and 5E), and identified molecular pathways enriched during *L. mexicana* infection, using PLS-DA (Figures 5F–5I). Both RAW 264.7 macrophages and BMDMs displayed distinct metabolic profiles in both the positive (Figures 5F and 5H) and negative (Figures 5G and 5I) mode datasets.

L. mexicana infection leads to enrichment of purine metabolites with anti-nociceptive activities in immortalized and primary macrophages

We found enrichment of numerous metabolic pathways in infected RAW 264.7 macrophage and BMDMs, compared to uninfected controls, highlighting a metabolic shift during infection. In particular, we were interested in identifying any significantly enriched purine and AA/endocannabinoid metabolites. Both RAW 264.7 macrophages and the BMDMs showed an enrichment of anti-nociceptive purine metabolites consistent with the results from the lesion tissue analysis (Figures 5J and 5K). Enrichment of purine metabolites with known anti-nociceptive activities, specifically inosine, xanthine, and hypoxanthine, are shown in Figure 5K. Our results showed no AA metabolism enrichment in either the RAW 264.7 macrophages or the BMDMs at 24 h post infection. These results identify macrophages as a source of anti-nociceptive purine metabolites during infection and potential players in *Leishmania*-mediated analgesia.

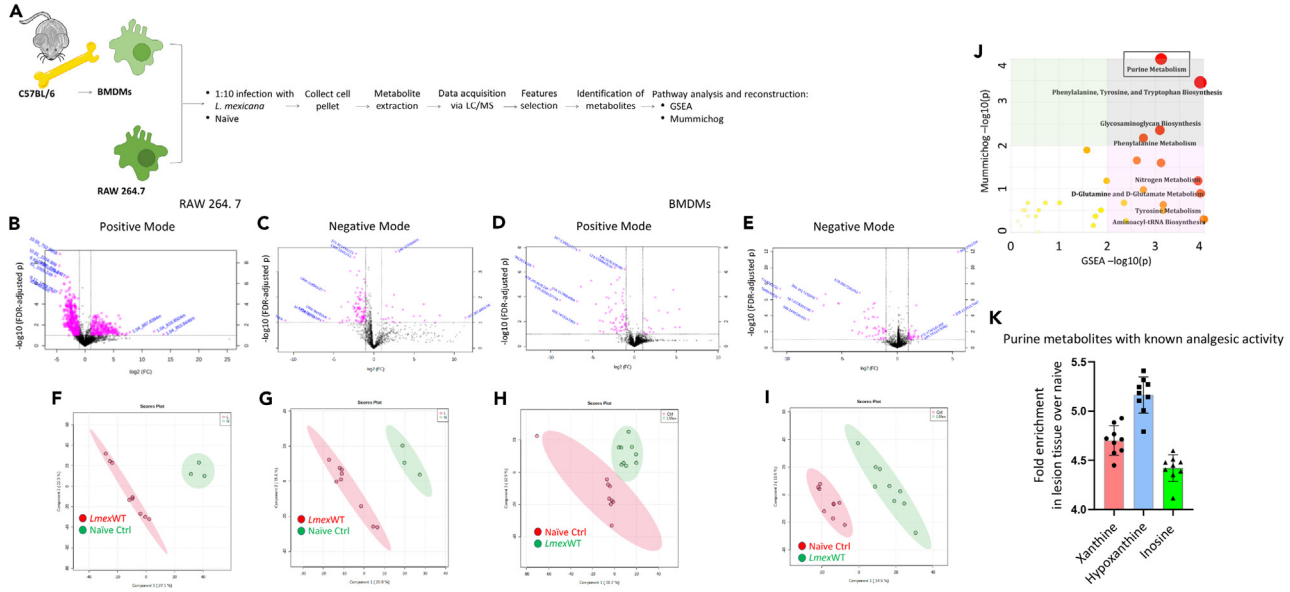

Figure 5. Experimental design for metabolomic analysis of analgesic pathways following *L. mexicana* infection

(A) Bone marrow-derived macrophages (BMDMs) derived from C57BL/6 mice, and RAW 264.7 macrophages were the infected with stationary phase *L. mexicana* parasites or treated with media (naive). After 24 h, the cell pellets were collected and processed for mass spectrometry. The data acquired were used to identify enriched metabolites and determine activated pathways in the tissue (n = 3 for each group with 3 experimental replicates for each group).

(B and C) Normalized data from RAW 264.7 macrophages or (D and E) BMDMs infected with *L. mexicana*, and naive controls was used to perform statistical analysis. (B and C) Features selected by volcano plot from positive and negative modes for cell pellets from RAW 264.7 macrophages or (D and E) BMDMs using LC/MS with fold change threshold (x) 2 and t-tests threshold (y) 0.05. Log transformed fold changes and p values are shown. PLS-DA from positive and negative modes for (F and G) RAW 264.7 macrophages and (H and I) BMDM cell pellets. Normalized data from RAW 264.7 macrophages or BMDMs infected with *L. mexicana* and naive control were used to perform integrated MS Peaks to Paths analysis.

(J) Results of the Fisher's method combining mummichog (y) and GSEA (x) p values from the RAW cell pellets in the positive mode datasets, indicating the enriched metabolic pathways is shown. The size and color of the circles correspond to their log-transformed combined p values. Large and red circles are considered the most perturbed pathways. The colored areas show the significant pathways based on either GSEA (pink) or mummichog (green), and the purple area in the upper right quadrant highlights significant pathways identified by both algorithms. Highlighted by a black box is purine metabolism found enriched in the dataset by both algorithms.

(K) Enrichment of purine metabolites in BMDMs infected with *L. mexicana* relative to naive in the positive mode dataset is shown.

In addition to purine metabolism and AA/endocannabinoid metabolism, our untargeted mass spectrometry analysis revealed up- or downregulation of several additional metabolites which are known to affect pain, based on previous studies. To definitively confirm the annotation of the metabolites such as histamine and prostaglandin E2 ethanolamide, known for anti- and pro-nociceptive properties, ear tissue extracts from the infected and naive control tissues were used to perform an untargeted LC/MS analysis alongside known standards to distinguish the isoforms of the metabolites. Spectra depicting the fragment masses (MS/MS) and the corresponding extracted ion chromatograms created by plotting the intensity of the signal observed at chosen m/z value for histamine (Figures 6A and 6B) showed a matching pattern between sample metabolites and the known standards. For prostaglandin E2 ethanolamide (Figures 6C, 6D and S1C), we detected a divergence between the main peak of the standard at 12.39 and the pooled sample. However, we detected a peak at 14.38 that matches with a corresponding smaller peak in the standard (highlighted in red dotted line Figure 6D), possibly suggesting the presence of the PGE2-EA isomer. The fold enrichment of these validated pro-nociceptive metabolites along with HMDB IDs, observed m/z ratios, and associated p values indicated that certain pro-nociceptive metabolites, such as histamine, are downregulated in the infected tissue, whereas prostaglandin E2 ethanolamide was enriched (Figure 6E).

DISCUSSION

CL patients, including those infected by *L. mexicana*, routinely report analgesia in their cutaneous lesions.[6–8] Other pathogens are also known to induce painless skin lesions, such as *Mycobacterium ulcerans*, the causative agent of Buruli ulcer,[34] and *Treponema pallidum*, the causative agent of syphilis.[35] On the other hand, lesions caused by *Staphylococcus aureus*,[9] *Herpes* virus,[10] and *Varicella zoster* virus[11] are painful. Taken together these observations indicate that pathogens may play a role in modulating nociception, either directly or indirectly, at the lesion site. Several studies have been conducted in the context of *Leishmania* and other pathogenic infections to determine the mechanisms responsible for pain, or lack of, at the lesion site. In particular, previous literature has focused on the role of cytokines. Just as pain neurons, called nociceptors, express protein channels to directly detect painful stimuli, they also have receptors for cytokines, lipid mediators, and other

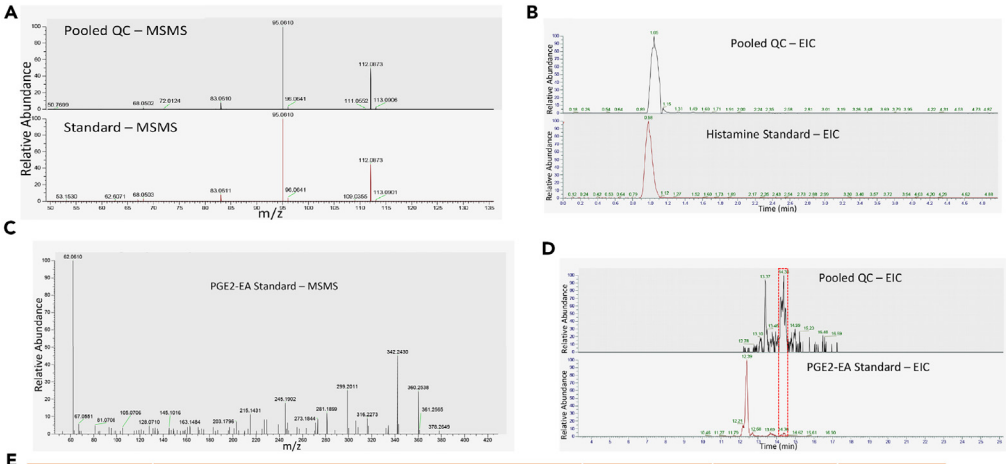

E

HMDB ID	Activity	Compound Name	m/z Ratio	Log (FC)
HMDB0000870	An amino-acid derived multi-functional neurotransmitter of the CNS and PNS that is released in response to tissue damage and contributes to pain hypersensitivity	Histamine	112.0873/1.03	-1.6226347
HMDB0013038	Endogenous eicosanoids resulting from the COX-2 metabolism of the endocannabinoid anandamide. It causes inflammatory pain by binding to its respective receptors in neurons, the EP receptor family, and subsequent activation of protein kinases and sensitization of TRPV1	Prostaglandin E2 ethanolamide	396.2745/14.35	0.7693991

Figure 6. Significant pro-nociceptive mediators found in *L. mexicana* infection compared to naive controls

To confirm the annotation of pronociceptive metabolites reported in the literature such as prostaglandin E2 ethanolamide and histamine, ear tissue extracts of infected and naive control were used to perform an untargeted LC/MS analysis alongside known standards to distinguish the isoform of the observed metabolites. Spectra depicting the fragment masses and the corresponding extracted ion chromatogram (EIC) that confirm a matching patterns between sample metabolites and the known standards are shown for histamine (A and B) and prostaglandin E2 ethanolamide (C and D). The confirmed m/z ratio, log fold change, and corresponding p value of the validated metabolites (E) show that certain pro-nociceptive metabolites, such as histamine, are downregulated in the infected tissue, while others, such as prostaglandin E2 ethanolamide, were enriched.

molecules released by immune cells during both acute and chronic inflammation. The interaction of these mediators with receptors on nociceptors can modulate the sensitivity of the neuron making it more or less likely to fire an action potential and relay the pain signal to the spinal cord and the brain.[22] Extensive evidence shows that pro-inflammatory cytokines such as IL-1β, IL-6, and TNF-α are involved in nociception[36] and can be found in *Staphylococcus aureus*[37] and *Varicella zoster* virus[38] infections associated with pain. However, the levels of IL-1β and TNF-α are also elevated in susceptible *L. mexicana* models,[39,40] characterized by lack of pain at the lesion site. This contradiction is further complicated by the conflicting results in previous studies of pre-clinical models of *L. major*-mediated anti-nociception.[16–21] The cytokine milieu, as well as the pain response in these studies varied greatly depending on the mouse model, inoculum, time point, and other factors.[16–21] Taken together these observations suggest that cytokines do not provide a complete picture of which mechanisms are responsible for CL-mediated analgesia, and that other mediators might be involved. After inoculation, *Leishmania* parasites reside within phagocytes such as macrophages.[1] It is well known that *Leishmania* can alter the metabolic profiles of infected cells including L-arginine metabolism and glycerophosphocholines.[41–49] These changes can modulate immunological functions in the host to promote parasitic survival.[41,43,50,51] However, the impact of this metabolic reprogramming on the lack of pain experienced by CL patients at the lesion site is unclear. In this study we were interested in using metabolomics approaches to investigate whether metabolic changes during the *L. mexicana* infection can modulate pain in cutaneous lesions and, in particular, the relationship between metabolic and immunological changes in the context of pain during leishmaniasis. We found the enrichment of several pathways with known anti-nociceptive properties in mice chronically infected with *L. mexicana*, as well as in infected macrophages *in vitro*. In particular, we found that several purine metabolites with anti-nociceptive activities were highly upregulated during infection. *Leishmania* parasites are purine auxotrophs and scavenge purine from the host cell in order to replicate,[52,53] therefore it is not surprising that infected host cells upregulate synthesis of purine metabolites such as the ones identified during infection *in vitro* and *in vivo*. In particular, *L. mexicana* parasites are known to utilize purine metabolites such as xanthine, hypoxanthine, and inosine as an energy source for cellular functions and replication.[54] Purine metabolites released by *L. mexicana*-infected macrophages could have modulatory paracrine functions on neighboring cells at the lesion site, as these metabolites are known to have multiple anti-inflammatory and immunomodulatory properties.[55–59] For instance, purines can induce an M2 immunosuppressive phenotype in macrophages, characterized by production of the cytokine IL-10, which is known to have anti-inflammatory and analgesic properties.[60,61] The role of IL-10 in susceptibility to *L. mexicana* has been previously described,[62,63] and this cytokine has been associated with hypoalgesia in *L. major*-infected BALB/c mice.[16] Furthermore, it is possible that in addition to promoting an anti-inflammatory environment permissive to *Leishmania* survival and replication, these purines could directly modulate nociception at the lesion site due to their action on adenosine receptors (ARs) on nociceptive neurons. Xanthine derivatives[59] and inosine[58] have been shown to have anti-nociceptive properties by acting through the ARs. ARs are

key regulators of inflammation and pain in nociceptors and other cells. In particular, signaling through A1R and A3R leads to a decrease in cAMP levels[55] and contributes to analgesia.[64–67] Purine metabolites can act on A1R and A3R to decrease nociception in sensory neurons by inhibiting excitatory Ca^{2+} currents,[64–66] and to impair transient receptor potential vanilloid (TRPV)-1 channel function indirectly by depleting PiP2 via A1R signaling, or directly by binding to TRPV1 channels.[64,65,67] TRPVs are non-selective Ca^{2+} channels responsible for sensing a wide range of painful stimuli and can mediate anti-nociception when inactivated or downregulated.[68,69] Taken together, these observations suggest that upregulated purine metabolism can result in increased production of anti-nociceptive cytokines, such as IL-10, and can also directly modulate pain at the lesion site by interacting with nociceptive neuronal receptors. Further analysis of mediators with known analgesic properties revealed upregulated metabolites of the AA pathway at the lesion site of infected mice, compared to naive mice. AA is a metabolite of AEA (NAE20:4 and NAE18:4) and 2-arachidonoylglycerol (2-AG), the two known endocannabinoids.[70] These functional lipids act on the cannabinoid receptors (CB) 1–2 to modulate different functions, including inflammation and pain.[24] CB1s reside throughout the central nervous system, while CB2s are mainly found in the peripheral nervous system and on immune cells.[71] Action through CBs leads to anti-nociception and suppression of pro-inflammatory cytokine production.[72] AEA specifically is a ligand for both CB1/CB2 and TRPV1, causing desensitization of TRPV1 at high concentrations.[73] Topical administration of cannabinoid compounds has been used for a long time to treat pain and has been validated in pre-clinical and clinical studies.[74–76] Furthermore, there is evidence of *Leishmania* infection modulating AA metabolism. In particular, infection with *L. donovani*, a visceral leishmaniasis strain, results in increased levels of AA in murine peritoneal macrophages.[77] AA is also the precursor of other biosynthetic pathways, such as the production of prostaglandins, thromboxane, and lipoxins which have been implicated in modulating inflammation and pain.[78,79] While prostaglandins and thromboxane can promote inflammation and nociception,[78,79] lipoxin A4 can lead to anti-nociception.[80] Based on these observations we hypothesize that *L. mexicana* infection can reduce inflammation and pain at the lesion site by upregulating the production of AA and endocannabinoid metabolites, resulting in the development of a parasite-permissive environment. The anti-nociceptive properties of endocannabinoids have been implicated not only in inflammatory pain, but also in chronic pain,[81] which could be a beneficial mechanism for *Leishmania* to utilize for long term survival. Interestingly, while we have shown upregulation of purine metabolism *in vitro*, we did not observe enriched AA metabolism in macrophages infected with *L. mexicana*. These results suggest that macrophages might not be the major source of AA/endocannabinoid metabolites in CL lesions, or that the *in vitro* nutrient milieu may not fully reflect the *in vivo* conditions. AA is found in the cell membrane phospholipids of many different cell types and stored in the lipid bodies of endothelial cells, fibroblasts, and immune cells such as macrophages, neutrophils, mast cells, and eosinophils.[82,83] Endocannabinoids are produced by neurons, as well as immune cells such as macrophages, basophils, and activated T and B cells.[84–86] Based on these observations, further research is necessary to determine the main source of AA and endocannabinoid mediators in CL lesions. Additionally, more studies are needed to determine whether the analgesic metabolites identified in this study are also present in physiologically relevant levels in human *L. mexicana* lesions, and whether they significantly contribute to the lack of pain experienced by CL patients. In this study we have focused on purine and AA metabolism due to their already established analgesic properties. However, our metabolomics analysis also revealed the enrichment of other pathways such as steroid hormones biosynthesis, catecholamine biosynthesis, nicotinate metabolism, and sphingolipid biosynthesis, which have also been implicated in pain modulation to some degree. Mice chronically infected with *L. mexicana* also showed upregulated palmitoleoyl ethanolamide, an endocannabinoid[87] with known anti-inflammatory effects. Interestingly, some of the anti-nociceptive mediators were also downregulated in infected samples, as shown by a negative LogFC. Furthermore, our analysis revealed the presence of pro-nociceptive mediators in our infected datasets, several of which, including histamine, were downregulated in infected samples. Taken all together, these results show a balance between pro- and anti-nociceptive mediators at the lesion site. Our future studies aim to elucidate the contribution of these pathways to analgesia in CL and determine whether they can interact synergistically to create an anti-inflammatory and anti-nociceptive environment at the lesion site. Overall, this study provides evidence of metabolic pathways upregulated in *L. mexicana* infection that have a known molecular basis for anti-nociceptive effects experienced by individuals infected with the parasite.

Limitations of the study

The biological activities of the metabolites associated with analgesia identified in this manuscript need to be experimentally validated in suitable experimental models. AEA 20:4, the most commonly reported endocannabinoid, was detected at a lower intensity than NAE 18:4. The MS/MS spectra for the PGE2-EA do not exactly agree with the standard presumably due to matrix effects on the standards or possibly multiple isoforms present in the PGE2-EA standard. The annotation of PGE2-EA is thus not as robust as it is for the other metabolites and is consistent with that of a PGE2-EA isomer.

STAR★METHODS

Detailed methods are provided in the online version of this paper and include the following:

- KEY RESOURCES TABLE
- RESOURCE AVAILABILITY
  - Lead contact
  - Materials availability
  - Data and code availability
- EXPERIMENTAL MODEL AND SUBJECT DETAILS

SUPPLEMENTAL INFORMATION

Supplemental information can be found online at https://doi.org/10.1016/j.isci.2023.108502.

ACKNOWLEDGMENTS

The authors thank the Campus Chemical Instrument Center (CCIC) Mass Spectrometry and Proteomics Facility at The Ohio State University (OSU) for their help. Our contributions are an informal communication and represent our own best judgment. These comments do not bind or obligate FDA.

AUTHOR CONTRIBUTIONS

G.V., S.G., H.L.N., and A.R.S. designed the experiments. G.V., B.C., M.B., and Y.M. performed the experiments. T.O., N.A., and M.B., analyzed the mass spectrometry data. G.V. and S.G. wrote the manuscript. G.V., T.O., B.C., Y.M., N.A., C.A., M.B., H.L.N, S.G, and A.R.S. revised the manuscript.

DECLARATION OF INTERESTS

This article reflects the views of the authors and should not be construed to represent FDA's views or policies. A.R.S. and The Ohio State University hold a patent #WO2012145734A1 entitled: "Antileishmanial compositions and methods of use".

Received: August 30, 2022
Revised: March 30, 2023
Accepted: November 17, 2023
Published: November 22, 2023

REFERENCES

1. McGwire, B.S., and Satoskar, A.R. (2014). Leishmaniasis: clinical syndromes and treatment. QJM *107*, 7–14.
2. World Health Organization, W. (2022). Leishmaniasis. https://www.who.int/news-room/fact-sheets/detail/leishmaniasis.
3. Volpedo, G., Pacheco-Fernandez, T., Holcomb, E.A., Cipriano, N., Cox, B., and Satoskar, A.R. (2021). Mechanisms of Immunopathogenesis in Cutaneous Leishmaniasis And Post Kala-azar Dermal Leishmaniasis (PKDL). Front. Cell. Infect. Microbiol. *11*, 685296.
4. Pace, D. (2014). Leishmaniasis. J. Infect. *69* (*Suppl 1*), S10–S18.
5. Kevric, I., Cappel, M.A., and Keeling, J.H. (2015). New World and Old World Leishmania Infections: A Practical Review. Dermatol. Clin. *33*, 579–593.
6. Borghi, S.M., Fattori, V., Conchon-Costa, I., Pinge-Filho, P., Pavanelli, W.R., and Verri, W.A., Jr. (2017). Leishmania infection: painful or painless? Parasitol. Res. *116*, 465–475.
7. Markle, W.H., and Makhoul, K. (2014). Cutaneous leishmaniasis: recognition and treatment. Am. Fam. Physician *69*, 1455–1460.
8. Andrade-Narváez, F.J., Vargas-González, A., Canto-Lara, S.B., and Damián-Centeno, A.G. (2001). Clinical picture of cutaneous leishmaniases due to Leishmania (Leishmania) mexicana in the Yucatan peninsula, Mexico. Mem. Inst. Oswaldo Cruz *96*, 163–167.
9. Centers for Disease Control and Prevention (2019). Methicillin-resistant Staphylococcus aureus (MRSA). https://www.cdc.gov/mrsa/community/index.html.
10. Centers for Disease Control and Prevention (2022). Genital Herpes – CDC Fact Sheet. https://www.cdc.gov/std/herpes/stdfact-herpes.htm#:~:text=Herpes%20sores%20usually%20appear%20as,occur%20during%20the%20first%20outbreak.
11. Centers for Disease Control and Prevention (2020). Shingles (Herpes Zoster). https://www.cdc.gov/shingles/hcp/clinical-overview.html.
12. González, U., Pinart, M., Reveiz, L., and Alvar, J. (2008). Interventions for Old World cutaneous leishmaniasis. Cochrane Database Syst. Rev. *8*, CD005067.
13. Wijnant, G.J., Van Bocxlaer, K., Fortes Francisco, A., Yardley, V., Harris, A., Alavijeh, M., Murdan, S., and Croft, S.L. (2018). Local Skin Inflammation in Cutaneous Leishmaniasis as a Source of Variable Pharmacokinetics and Therapeutic Efficacy of Liposomal Amphotericin B. Antimicrob. Agents Chemother. *62*, e00631-18.
14. Saldanha, M.G., Pagliari, C., Queiroz, A., Machado, P.R.L., Carvalho, L., Scott, P., Carvalho, E.M., and Arruda, S. (2020). Tissue Damage in Human Cutaneous Leishmaniasis: Correlations Between Inflammatory Cells and Molecule Expression. Front. Cell. Infect. Microbiol. *10*, 355.
15. Antonio, L.d.F., Lyra, M.R., Saheki, M.N., Schubach, A.d.O., Miranda, L.d.F.C., Madeira, M.d.F., Lourenço, M.C.d.S., Fagundes, A., Ribeiro, É.A.D.S., Barreto, L., and Pimentel, M.I.F. (2017). Effect of secondary infection on epithelialisation and total healing of cutaneous leishmaniasis lesions. Mem. Inst. Oswaldo Cruz *112*, 640–646.
16. Cangussú, S.D., Souza, C.C., Castro, M.S.A., Vieira, L.Q., Cunha, F.Q., Afonso, L.C.C., and Arantes, R.M.E. (2013). The endogenous cytokine profile and nerve fibre density in mouse ear Leishmania major-induced lesions

related to nociceptive thresholds. Exp. Parasitol. *133*, 193–200.
17. Kanaan, S.A., Saadé, N.E., Karam, M., Khansa, H., Jabbur, S.J., and Jurjus, A.R. (2000). Hyperalgesia and upregulation of cytokines and nerve growth factor by cutaneous leishmaniasis in mice. Pain *85*, 477–482.
18. Karam, M.C., Hamdan, H.G., Abi Chedid, N.A., Bodman-Smith, K.B., Eales-Reynolds, L.J.E., and Baroody, G.M. (2006). Leishmania major: low infection dose causes short-lived hyperalgesia and cytokines upregulation in mice. Exp. Parasitol. *113*, 168–173.
19. Karam, M.C., Merckbawi, R., El-Kouba, J.E., Bazzi, S.I., and Bodman-Smith, K.B. (2013). In Leishmania major-induced inflammation, interleukin-13 reduces hyperalgesia, down-regulates IL-1β and up-regulates IL-6 in an IL-4 independent mechanism. Exp. Parasitol. *134*, 200–205.
20. Haber, M.E., Daher, C.F., Karam, M.C., and Baroody, G.M. (2009). Leishmania major: interleukin-13 increases the infection-induced hyperalgesia and the levels of interleukin- 1beta and interleukin-12 in rats. Exp. Parasitol. *121*, 224–229.
21. Mantyh, P.W., Allen, C.J., Rogers, S., DeMaster, E., Ghilardi, J.R., Mosconi, T., Kruger, L., Mannon, P.J., Taylor, I.L., and Vigna, S.R. (1994). Some sensory neurons express neuropeptide Y receptors: potential paracrine inhibition of primary afferent nociceptors following peripheral nerve injury. J. Neurosci. *14*, 3958–3968.
22. Bennett, D.L., Clark, A.J., Huang, J., Waxman, S.G., and Dib-Hajj, S.D. (2019). The Role of Voltage-Gated Sodium Channels in Pain Signaling. Physiol. Rev. *99*, 1079–1151.
23. Binshtok, A.M. (2011). Mechanisms of nociceptive transduction and transmission: a machinery for pain sensation and tools for selective analgesia. Int. Rev. Neurobiol. *97*, 143–177.
24. Barrie, N., and Manolios, N. (2017). The endocannabinoid system in pain and inflammation: Its relevance to rheumatic disease. Eur. J. Rheumatol. *4*, 210–218.
25. Wei, J., Su, W., Zhao, Y., Wei, Z., Hua, Y., Xue, P., Zhu, X., Chen, Y., and Chen, G. (2022). Maresin 1 promotes nerve regeneration and alleviates neuropathic pain after nerve injury. J. Neuroinflammation *19*, 32.
26. Serhan, C.N., Dalli, J., Colas, R.A., Winkler, J.W., and Chiang, N. (2015). Protectins and maresins: New pro-resolving families of mediators in acute inflammation and resolution bioactive metabolome. Biochim. Biophys. Acta *1851*, 397–413.
27. Martini, A.C., Berta, T., Forner, S., Chen, G., Bento, A.F., Ji, R.R., and Rae, G.A. (2016). Lipoxin A4 inhibits microglial activation and reduces neuroinflammation and neuropathic pain after spinal cord hemisection. J. Neuroinflammation *13*, 75.
28. Scorza, B.M., Carvalho, E.M., and Wilson, M.E. (2017). Cutaneous Manifestations of Human and Murine Leishmaniasis. Int. J. Mol. Sci. *18*, 1296.
29. Gabriel, Á., Valério-Bolas, A., Palma-Marques, J., Mourata-Gonçalves, P., Ruas, P., Dias-Guerreiro, T., and Santos-Gomes, G. (2019). Cutaneous Leishmaniasis: The Complexity of Host's Effective Immune Response against a Polymorphic Parasitic Disease. J. Immunol. Res. *2019*, 2603730.
30. Contreras, I., Estrada, J.A., Guak, H., Martel, C., Borjian, A., Ralph, B., Shio, M.T., Fournier, S., Krawczyk, C.M., and Olivier, M. (2014). Impact of Leishmania mexicana infection on dendritic cell signaling and functions. PLoS Negl. Trop. Dis. *8*, e3202.
31. Hsu, A.C., and Scott, P. (2007). Leishmania mexicana infection induces impaired lymph node expansion and Th1 cell differentiation despite normal T cell proliferation. J. Immunol. *179*, 8200–8207.
32. Marion, E., Song, O.R., Christophe, T., Babonneau, J., Fenistein, D., Eyer, J., Letournel, F., Henrion, D., Clere, N., Paille, V., et al. (2014). Mycobacterial toxin induces analgesia in buruli ulcer by targeting the angiotensin pathways. Cell *157*, 1565–1576.
33. Kirchner, J.T. (1991). Syphilis–an STD on the increase. Am. Fam. Physician *44*, 843–854.
34. Wang, J.P., Kurt-Jones, E.A., Shin, O.S., Manchak, M.D., Levin, M.J., and Finberg, R.W. (2005). Varicella-zoster virus activates inflammatory cytokines in human monocytes and macrophages via Toll-like receptor 2. J. Virol. *79*, 12658–12666.
35. Fernández-Figueroa, E.A., Rangel-Escareño, C., Espinosa-Mateos, V., Carrillo-Sánchez, K., Salaiza-Suazo, N., Carrada-Figueroa, G., March-Mifsut, S., and Becker, I. (2012). Disease severity in patients infected with Leishmania mexicana relates to IL-1β. PLoS Negl. Trop. Dis. *6*, e1533.
36. Satoskar, A., and Alexander, J. (1995). Sex-determined susceptibility and differential IFN-gamma and TNF-alpha mRNA expression in DBA/2 mice infected with Leishmania mexicana. Immunology *84*, 1–4.
37. Volpedo, G., Pacheco-Fernandez, T., Bhattacharya, P., Oljuskin, T., Dey, R., Gannavaram, S., Satoskar, A.R., and Nakhasi, H.L. (2021). Determinants of Innate Immunity in Visceral Leishmaniasis and Their Implication in Vaccine Development. Front. Immunol. *12*, 748325.
38. Saunders, E.C., and McConville, M.J. (2020). Immunometabolism of Leishmania granulomas. Immunol. Cell Biol. *98*, 832–844.
39. Naderer, T., Heng, J., Saunders, E.C., Kloehn, J., Rupasinghe, T.W., Brown, T.J., and McConville, M.J. (2015). Intracellular Survival of Leishmania major Depends on Uptake and Degradation of Extracellular Matrix Glycosaminoglycans by Macrophages. PLoS Pathog. *11*, e1005136.
40. Reverte, M., Eren, R.O., Jha, B., Desponds, C., Snäkä, T., Prevel, F., Isorce, N., Lye, L.F., Owens, K.L., Gazos Lopes, U., et al. (2021). The antioxidant response favors Leishmania parasites survival, limits inflammation and reprograms the host cell metabolism. PLoS Pathog. *17*, e1009422.
41. Kloehn, J., Blume, M., Cobbold, S.A., Saunders, E.C., Dagley, M.J., and McConville, M.J. (2016). Using metabolomics to dissect host-parasite interactions. Curr. Opin. Microbiol. *32*, 59–65.
42. Martin, J.L., Yates, P.A., Soysa, R., Alfaro, J.F., Yang, F., Burnum-Johnson, K.E., Petyuk, V.A., Weitz, K.K., Camp, D.G., 2nd, Smith, R.D., et al. (2014). Metabolic reprogramming during purine stress in the protozoan pathogen Leishmania donovani. PLoS Pathog. *10*, e1003938.
43. Sopwith, W.F., Debrabant, A., Yamage, M., Dwyer, D.M., and Bates, P.A. (2002). Developmentally regulated expression of a cell surface class I nuclease in Leishmania mexicana. Int. J. Parasitol. *32*, 449–459.
44. Kloehn, J., Boughton, B.A., Saunders, E.C., O'Callaghan, S., Binger, K.J., and McConville, M.J. (2021). Identification of Metabolically Quiescent Leishmania mexicana Parasites in Peripheral and Cured Dermal Granulomas Using Stable Isotope Tracing Imaging Mass Spectrometry. mBio *12*, e00129-21.
45. Lamour, S.D., Choi, B.S., Keun, H.C., Müller, I., and Saric, J. (2012). Metabolic characterization of Leishmania major infection in activated and nonactivated macrophages. J. Proteome Res. *11*, 4211–4222.
46. Muxel, S.M., Mamani-Huanca, M., Aoki, J.I., Zampieri, R.A., Floeter-Winter, L.M., López-Gonzálvez, Á., and Barbas, C. (2019). Metabolomic Profile of BALB/c Macrophages Infected with Leishmania amazonensis: Deciphering L-Arginine Metabolism. Int. J. Mol. Sci. *20*, 6248.
47. Parab, A.R., Thomas, D., Lostracco-Johnson, S., Siqueira-Neto, J.L., McKerrow, J.H., Dorrestein, P.C., and McCall, L.I. (2021). Dysregulation of Glycerophosphocholines in the Cutaneous Lesion Caused by Leishmania major in Experimental Murine Models. Pathogens *10*, 593.
48. Saunders, E.C., Ng, W.W., Kloehn, J., Chambers, J.M., Ng, M., and McConville, M.J. (2014). Induction of a stringent metabolic response in intracellular stages of Leishmania mexicana leads to increased dependence on mitochondrial metabolism. PLoS Pathog. *10*, e1003888.
49. Vargas, D.A., Prieto, M.D., Martínez-Valencia, A.J., Cossio, A., Burgess, K.E.V., Burchmore, R.J.S., and Gómez, M.A. (2019). Pharmacometabolomics of Meglumine Antimoniate in Patients With Cutaneous Leishmaniasis. Front. Pharmacol. *10*, 657.
50. Hassan, H.F., and Coombs, G.H. (1985). Leishmania mexicana: purine-metabolizing enzymes of amastigotes and promastigotes. Exp. Parasitol. *59*, 139–150.
51. Welihinda, A.A., Kaur, M., Greene, K., Zhai, Y., and Amento, E.P. (2016). The adenosine metabolite inosine is a functional agonist of the adenosine A2A receptor with a unique signaling bias. Cell. Signal. *28*, 552–560.
52. Zylka, M.J. (2010). Needling adenosine receptors for pain relief. Nat. Neurosci. *13*, 783–784.
53. Yamaoka, G., Horiuchi, H., Morino, T., Miura, H., and Ogata, T. (2013). Different analgesic effects of adenosine between postoperative and neuropathic pain. J. Orthop. Sci. *18*, 130–136.
54. Nascimento, F.P., Macedo-Júnior, S.J., Pamplona, F.A., Luiz-Cerutti, M., Córdova, M.M., Constantino, L., Tasca, C.I., Dutra, R.C., Calixto, J.B., Reid, A., et al. (2015). Adenosine A1 receptor-dependent antinociception induced by inosine in mice: pharmacological, genetic and biochemical aspects. Mol. Neurobiol. *51*, 1368–1378.
55. Zygmunt, M., Sapa, J., Drabczyńska, A., Karcz, T., Müller, C., Köse, M., Latacz, G., Schabikowski, J., Bednarski, M., and Kieć-Kononowicz, K. (2015). Synthesis and Analgesic Activity of Annelated Xanthine Derivatives in Experimental Models in Rodents. Arch. Pharm. (Weinheim) *348*, 704–714.
56. Laumet, G., Bavencoffe, A., Edralin, J.D., Huo, X.J., Walters, E.T., Dantzer, R., Heijnen, C.J., and Kavelaars, A. (2020). Interleukin-10 resolves pain hypersensitivity induced by cisplatin by reversing sensory neuron hyperexcitability. Pain *161*, 2344–2352.
57. Ohradanova-Repic, A., Machacek, C., Charvet, C., Lager, F., Le Roux, D., Platzer, R., Leksa, V., Mitulovic, G., Burkard, T.R., Zlabinger, G.J., et al. (2018). Extracellular Purine Metabolism Is the Switchboard of

Immunosuppressive Macrophages and a Novel Target to Treat Diseases With Macrophage Imbalances. Front. Immunol. *9*, 852.
58. Padigel, U.M., Alexander, J., and Farrell, J.P. (2003). The role of interleukin-10 in susceptibility of BALB/c mice to infection with Leishmania mexicana and Leishmania amazonensis. J. Immunol. *171*, 3705–3710.
59. Buxbaum, L.U., and Scott, P. (2005). Interleukin 10- and Fcgamma receptor-deficient mice resolve Leishmania mexicana lesions. Infect. Immun. *73*, 2101–2108.
60. Sowa, N.A., Street, S.E., Vihko, P., and Zylka, M.J. (2010). Prostatic acid phosphatase reduces thermal sensitivity and chronic pain sensitization by depleting phosphatidylinositol 4,5- bisphosphate. J. Neurosci. *30*, 10282–10293.
61. Chen, W.H., Tzen, J.T.C., Hsieh, C.L., Chen, Y.H., Lin, T.J., Chen, S.Y., and Lin, Y.W. (2012). Attenuation of TRPV1 and TRPV4 Expression and Function in Mouse Inflammatory Pain Models Using Electroacupuncture. Evid. Based. Complement. Alternat. Med. *2012*, 636848.
62. Coppi, E., Cherchi, F., Fusco, I., Failli, P., Vona, A., Dettori, I., Gaviano, L., Lucarini, E., Jacobson, K.A., Tosh, D.K., et al. (2019). Adenosine A3 receptor activation inhibits pronociceptive N-type Ca2+ currents and cell excitability in dorsal root ganglion neurons. Pain *160*, 1103–1118.
63. Puntambekar, P., Van Buren, J., Raisinghani, M., Premkumar, L.S., and Ramkumar, V. (2004). Direct interaction of adenosine with the TRPV1 channel protein. J. Neurosci. *24*, 3663–3671.
64. Kumamoto, E., Fujita, T., and Jiang, C.Y. (2014). TRP Channels Involved in Spontaneous L- Glutamate Release Enhancement in the Adult Rat Spinal Substantia Gelatinosa. Cells *3*, 331–362.
65. Nilius, B., and Owsianik, G. (2011). The transient receptor potential family of ion channels. Genome Biol. *12*, 218.
66. Maccarrone, M. (2017). Metabolism of the Endocannabinoid Anandamide: Open Questions after 25 Years. Front. Mol. Neurosci. *10*, 166.
67. Seltzman, H.H., Shiner, C., Hirt, E.E., Gilliam, A.F., Thomas, B.F., Maitra, R., Snyder, R., Black, S.L., Patel, P.R., Mulpuri, Y., and Spigelman, I. (2016). Peripherally Selective Cannabinoid 1 Receptor (CB1R) Agonists for the Treatment of Neuropathic Pain. J. Med. Chem. *59*, 7525–7543.
68. Amaya, F., Shimosato, G., Kawasaki, Y., Hashimoto, S., Tanaka, Y., Ji, R.R., and Tanaka, M. (2006). Induction of CB1 cannabinoid receptor by inflammation in primary afferent neurons facilitates antihyperalgesic effect of peripheral CB1 agonist. Pain *124*, 175–183.
69. Singh Tahim, A., Sántha, P., and Nagy, I. (2005). Inflammatory mediators convert anandamide into a potent activator of the vanilloid type 1 transient receptor potential receptor in nociceptive primary sensory neurons. Neuroscience *136*, 539–548.
70. Dogrul, A., Gul, H., Akar, A., Yildiz, O., Bilgin, F., and Guzeldemir, E. (2003). Topical cannabinoid antinociception: synergy with spinal sites. Pain *105*, 11–16.
71. Maida, V., and Corban, J. (2017). Topical Medical Cannabis: A New Treatment for Wound Pain- Three Cases of Pyoderma Gangrenosum. J. Pain Symptom Manage. *54*, 732–736.
72. Xu, D.H., Cullen, B.D., Tang, M., and Fang, Y. (2020). The Effectiveness of Topical Cannabidiol Oil in Symptomatic Relief of Peripheral Neuropathy of the Lower Extremities. Curr. Pharm. Biotechnol. *21*, 390–402.
73. Reiner, N.E., and Malemud, C.J. (1985). Arachidonic acid metabolism by murine peritoneal macrophages infected with Leishmania donovani: in vitro evidence for parasite-induced alterations in cyclooxygenase and lipoxygenase pathways. J. Immunol. *134*, 556–563.
74. Chandrasekharan, J.A., and Sharma-Walia, N. (2015). Lipoxins: nature's way to resolve inflammation. J. Inflamm. Res. *8*, 181–192.
75. Ferreira, S.H., Moncada, S., and Vane, J.R. (1997). Prostaglandins and the mechanism of analgesia produced by aspirin-like drugs. 1973. Br. J. Pharmacol. *120*, 401–412. discussion 399-400.
76. Kinsey, S.G., Long, J.Z., Cravatt, B.F., and Lichtman, A.H. (2010). Fatty acid amide hydrolase and monoacylglycerol lipase inhibitors produce anti-allodynic effects in mice through distinct cannabinoid receptor mechanisms. J. Pain *11*, 1420–1428.
77. Tallima, H., and El Ridi, R. (2018). Arachidonic acid: Physiological roles and potential health benefits - A review. J. Adv. Res. *11*, 33–41.
78. Weller, P.F. (2016). Leukocyte lipid bodies - structure and function as "eicosasomes". Trans. Am. Clin. Climatol. Assoc. *127*, 328–340.
79. Navarrete, M., Díez, A., and Araque, A. (2014). Astrocytes in endocannabinoid signalling. Philos. Trans. R. Soc. Lond. B Biol. Sci. *369*, 20130599.
80. Pandey, R., Mousawy, K., Nagarkatti, M., and Nagarkatti, P. (2009). Endocannabinoids and immune regulation. Pharmacol. Res. *60*, 85–92.
81. Sido, J.M., Nagarkatti, P.S., and Nagarkatti, M. (2016). Production of endocannabinoids by activated T cells and B cells modulates inflammation associated with delayed-type hypersensitivity. Eur. J. Immunol. *46*, 1472–1479.
82. Peritore, A.F., Siracusa, R., Crupi, R., and Cuzzocrea, S. (2019). Therapeutic Efficacy of Palmitoylethanolamide and Its New Formulations in Synergy with Different Antioxidant Molecules Present in Diets. Nutrients *11*, 2175.
83. The University of Manchester, and MIB Biospec Group Laboratory Guide for Metabolomic Experiments. www.biospec.net/wordpress/wp-content/uploads/Metabolomics-laboratory-handbook.pdf.
84. Piomelli, D., and Sasso, O. (2014). Peripheral gating of pain signals by endogenous lipid mediators. Nat. Neurosci. *17*, 164–174.
85. Raja, S.N. (1998). Peripheral modulatory effects of catecholamines in inflammatory and neuropathic pain. Adv. Pharmacol. *42*, 567–571.
86. Obara, I., Telezhkin, V., Alrashdi, I., and Chazot, P.L. (2020). Histamine, histamine receptors, and neuropathic pain relief. Br. J. Pharmacol. *177*, 580–599.
87. Shelnut, E.L., Nikas, S.P., Finnegan, D.F., Chiang, N., Serhan, C.N., and Makriyannis, A. (2015). Design and synthesis of novel prostaglandin E. Tetrahedron Lett. *56*, 1411–1415.

STAR★METHODS

KEY RESOURCES TABLE

REAGENT or RESOURCE	SOURCE	IDENTIFIER
Experimental models: Organisms/strains		
Leishmania mexicana WT	N/A	MNYC/B2/62/m379
RAW264.7	ATCC	TIB-71; RRID: CVCL_0493
Software and algorithms		
MetaboAnalyst 4.0.	Chong et al.[59]	https://www.metaboanalyst.ca/home.xhtml
Metscape	Karnovsky et al.[30]	http://metscape.ncibi.org/
Kyoto Encyclopedia of Genes and Genomes (KEGG)	Kanehisa et al.[60]	https://www.genome.jp/kegg/
Graph Pad Prism 9	Dotmatics	https://www.graphpad.com/
Progenesis QI	Nonlinear Dynamics	https://www.nonlinear.com/progenesis/qi/v1.0/faq/compound-search-metascope.aspx
Other		
Q-Exactive Plus Orbitrap mass spectrometer	Thermo Scientific	IQLAAEGAAPFALGMBDK
Deposited data		
Metabolomic data	National Metabolomics Data Repository	https://doi.org/10.21228/M8FT6G

RESOURCE AVAILABILITY

Lead contact

Further information and requests for resources and reagents should be directed to and will be fulfilled by the Lead Contact and Corresponding Author, Dr. Abhay R. Satoskar (abhay.satoskar@osumc.edu).

Materials availability

This study did not generate new unique reagents.

Data and code availability

All relevant data is available in the main text and supplementary information. The metabolomics data is available at the Databse: NIH Common Fund's National Metabolomics Data Repository (NMDR), the Metabolomics Workbench, https://www.metabolomicsworkbench.org where it has been assigned Project ID (http://dev.metabolomicsworkbench.org:22222/data/DRCCMetadata.php?Mode=Study&StudyID=ST002974&Access=JzwI9127). The data can be accessed directly via it's Project DOI: (https://doi.org/10.21228/M8FT6G).

This work is supported by Metabolomics Workbench/National Metabolomics Data Repository (NMDR) (grant# U2C-DK119886), Common Fund Data Ecosystem (CFDE) (grant# 3OT2OD030544) and Metabolomics Consortium Coordinating Center (M3C) (grant# 1U2C-DK119889).
This paper does not report original code. Any additional information can be provided by the lead contact upon reasonable request.

EXPERIMENTAL MODEL AND SUBJECT DETAILS

Mice

Female C57BL/6 mice were purchased from Envigo (Harlan laboratories) Indianapolis, IN, USA, and housed at The Ohio State University animal facility, following approved animal protocols and University Laboratory Animal Resources (ULAR) regulations (2010A0048-R3 Protocol). All the experiments were performed using 5 age-matched 5-8 week old female mice per group. 129S6/SvEvTac mice were purchased from Taconic Biosciences, Inc.

Parasites

129S/SvEvTac mice were used to maintain L. mexicana (MNYC/B2/62/m379) parasites via subcutaneous inoculation into the shaved back rumps. Amastigotes were then obtained from the draining lymph nodes of infected mice and grown at 26°C in M199 medium supplemented with 1% Penicillin/Streptomycin, and 1% HEPES 10% fetal bovine serum (FBS), to generate stationary phase promastigotes.

BMDMs and RAW cells for *in vitro* studies we used the immortalized RAW 264.7 macrophage cell line, as well as primary bone marrow-derived macrophages (BMDMs). The RAW 264.7 cell line was purchased from American Type Culture Collection (ATCC), and cell identity

was verified regularly based on cell morphology. Both RAW 264.7 and BMDMs were cultured with RPMI medium supplemented with 10% fetal bovine serum (FBS), 1% penicillin/streptomycin and 1% HEPES at 37°C with 5% CO2. BMDMs were obtained from the femur and tibias of C57BL/6 mice. After isolation, the bone marrow was cultured with complete RPMI supplemented with 20% supernatant from L-929 cells for 7-10 days until differentiation was complete.

METHOD DETAILS

In vitro cell culture and infection

RAW 264.7 macrophages and BMDMs were plated in a 24-well plate at a density of 0.5x106 per well and infected overnight with stationary phase *L. mexicana* promastigotes at a ratio of 10:1 (parasite to macrophages). The controls were treated with media alone. Then, the extracellular parasites were removed by washing with PBS and new media was applied. After a 24hrs incubation, the supernatant and cell pellet were collected and processed for mass spectrometry.

Mass spectrometry

For *in vitro* experiments, the culture supernatant was collected and cell debris was removed by centrifugation according to SOP 5 of the Laboratory Guide for Metabolomics Experiments.[83] The attached cells were be scraped, washed with PBS and quenched with 80% methanol. Then they were snap-frozen, centrifuged, and lyophilized according to SOP 4 of the Laboratory Guide for Metabolomics Experiments.[83] For *in vivo* studies, the ears were collected, snap frozen, and processed for mass spectrometry analysis according to SOP 7 of the Laboratory Guide for Metabolomics Experiments.[83] Samples were then incubated with 500 uL of 100% MeOH and sonicated. The tissue was weighed and homogenized at 40 mg/mL of 50% MeOH solution for 3 cycles in a Precellys homogenizer. The supernatant was collected, dried down, and reconstituted in ½ of the original volume in 5 % MeOH with 0.1 % formic acid. For metabolite candidates found via untargeted analysis, pure standards purchased from Sigma-Aldrich were diluted in 100 % MeOH stocks to 10 ug/mL, dried down, and reconstituted in 5% MeOH with 0.1% formic acid and run in the same conditions described below to match features for identification. Untargeted analysis was performed on a Thermo Scientific Q-Exactive Plus Orbitrap mass spectrometer (MS) with HPLC separation on a Poroshell 120 SB-C18 (2 x 100 mm, 2.7 μm particle size) with a Thermo Scientific Ultimate WPS 3000 UHPLC system. The gradient consisted of solvent A, H2O with 0.1% Formic acid, and solvent B 100% acetonitrile at a 200 μL/min flow rate with an initial 2% solvent B with a linear ramp to 95% B at 15 min, holding at 95% B for 1 minutes, and back to 5% B from 17 min and equilibration of 5% B until min 30. For each sample, 5 μL was injected for each sample with ionization in the MS on a HESI electrospray ionization source using a capillary voltage of 4.5 kV in positive and 4.0 kV in negative mode at 320 °C capillary temperature and 100 °C probe temperature. Gas settings were set to 15 for sheath gas and 5 auxiliary gas while the S-Lens was set to 50 V. The top 5 ions were selected for data dependent analysis with a 10 second exclusion window, with a mass range of 80-1200 m/z and a resolution of 70,000 for MS scans and 17,5000 for MSMS scans and fragmentation normalized collision energies of 30 V. For feature selection in the untargeted results analysis, including database comparison and statistical processing, samples were analyzed in Progenesis QI and the pooled sample runs were selected for feature alignment. Using the pooled QC samples, features with above 30% CV and max abundances below 5000 intensity were filtered out and Anova p-value scores between the groups were calculated with a cutoff of < 0.05. With database matching using the Human Metabolome Database, selecting for adducts M+H, M+Na, M+2H, and 2M+H for positive mode and M-H, M+Cl, M-2H, and 2M-H and less than 10 ppm mass error, unique features were tentatively identified as potential metabolites. Metabolites were only annotated with MSMS fragmentation matching scores above 20% with Progenesis Metascope.

QUANTIFICATION AND STATISTICAL ANALYSIS

Statistical analysis of mass spectrometry datasets

Peak intensity data tables from the mass spectrometry experiment were formatted into comma-separated values (CSV) files conforming to MetaboAnalyst's requirements and uploaded into the one-factor statistical analysis module. Each analysis passed MetaboAnalyst's internal data integrity check and additional data filtering was performed based on interquartile range. On the normalization overview page, sample normalization was performed based on the median of the data and the auto-scaling option was chosen to perform data scaling; No transformation of the data was performed. For dimensionality reduction, both principal component analysis (PCA) and partial least-squares discriminant analysis (PLSDA) were employed. Cross-validated sum of squares (Q2) performance measures were used to determine if PLSDA models were overfitted. Visualization of significant, differentially regulated metabolites was done by generating volcano plots with cutoffs of <0.05 false-discovery rate (FDR) and > 2-fold change (FC). Clustering of samples and features were analyzed by creating dendrograms and hierarchical heatmaps, respectively.

Pathway analysis of mass spectrometry datasets

We have used two different techniques in order to identify enriched pathways in our data sets. First we used the Functional Analysis Module (MS peaks to pathways) in MetaboAnalyst 4.0. Detected peaks (mass-to-charge ratios + retention times) from positive and negative analytical modes of the mass spectrometer for each sample were organized into four column lists along with calculated FDR-corrected *p*-values and t-scores from univariate t-tests. These peak list profiles were uploaded to the functional analysis module and passed the internal data integrity checks. The ion mode in MetaboAnalyst was set to the appropriate type depending on the analytical mode that was used to generate the data. For each analysis the mass tolerance was set to 10 ppm, the retention time units were set to minutes, and the option to enforce primary

ions was checked. In parameter settings, the mummichog algorithm (version 2.0) and the modified gene set enrichment algorithm were used for all analyses. The *p*-value cutoff for the mummichog algorithm was left at the default (top 10% of peaks). Currency metabolites and adducts were left at default settings. Lastly, the Kyoto Encyclopedia of Genes and Genomes (KEGG) pathway library for *Mus musculus* was selected as the metabolic network that the functional analysis module would use to infer pathway activity and predict metabolite identity; only pathways/metabolite sets with at least three entries were allowed.

Integrative network analysis

The Metscape 3.1.3 App from the Cytoscape 3.9.1 software was used in order to build integrative network analysis of our in-vivo dataset using Metscape's internal database which incorporates KEGG and EHMN data. The IDs of the metabolomic dataset were converted from HMDB IDs to KEGG IDs recognized by the Cytoscape software via the Chemical Translation Service (CTS) and verified by the Metaboanalyst Compound ID Conversion tool. The metabolomic dataset was then uploaded as a compound file to Metscape and the FDR-adjusted *p*- Value and FC Ratio cutoff points were set at 0.05 and 1.5 respectively. 810 from a total of 2771 metabolites were not accepted as input compounds by Metscape and were removed from the dataset. A Compound-compound network was created for the detected purine Metabolism pathway of our dataset, along with an integrative network build from the combination of arachidonic acid Metabolism, glycerophospholipid metabolism, linoleate metabolism, and prostaglandin formation from arachidonate. The two created networks allowed us to visualize the integrated relationship among the metabolites and endocannabinoids involved in purine metabolism and arachidonic acid metabolism respectively.

Statistical analysis

All *in vitro* and *in vivo* data show a representative experiment with N =3 per group, with 4 experimental replicates in each group. N represents different biological replicates. For the mass spectrometry data all statistical analysis were performed with MetaboAnalyst software.

ADDITIONAL RESOURCES

The authors did not utilize any additional resources.